THE JOURNAL OF PHYSICAL CHEMISTRY C

Article

Cite This: J. Phys. Chem. C 2019, 123, 1596−1601

pubs.acs.org/JPCC

Electrical Double Layers Close to Ionic Liquid−Solvent Demixing

Carolina Cruz,[†] Alina Ciach,*[,†] Enrique Lomba,[‡] and Svyatoslav Kondrat*[,†]

[†]Department of Complex Systems, Institute of Physical Chemistry PAS, Warsaw 01-224, Poland

[‡]Institute of Physical Chemistry Rocasolano, CSIC, Madrid 28006, Spain

ABSTRACT: Electrical double layers (EDLs) play a key role in energy storage and have been suggested to have applications in energy generation. Recently, there has been an expansion of interest in EDLs, but EDLs with ionic liquid−solvent mixtures (ILSMs) received less attention. Herein, we study the temperature dependence of EDLs with ILSMs, in particular, close to demixing. We demonstrate the emergence of a bird-shaped capacitance, in addition to the well-known camel and bell shapes, which manifests the fine interplay between the electrostatic and wetting properties of ILSMs. We find that the capacitance increases appreciably as the system approaches demixing and this increase is accompanied by a sizeable enhancement of the energy storage, which can be utilized for generating electricity from waste heat.

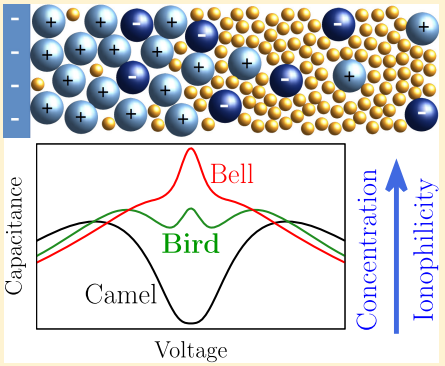

INTRODUCTION

The last decades witnessed an explosion of interest in properties of ionic liquids (ILs) and ionic liquid solutions. Room-temperature ILs have large electrochemical windows, low vapor pressure, and high thermal stability,[1,2] finding their applications in numerous fields, such as energy storage and generation,[3−6] lubrication,[7] catalysis,[8,9] etc. One of the key applications is in electrical double-layer capacitors, also known as supercapacitors or ultracapacitors, which store energy by a potential-driven accumulation of countercharge in an electrical double layer (EDL), formed at an IL−electrode interface.[10] Theories developed for EDLs have demonstrated that excluded-volume (steric) interactions are essential to describe the EDL properties.[11−18] Steric interactions were shown to lead to the so-called camel and bell-shape capacitances, obtained at low and high IL concentrations, respectively, instead of the U-shaped capacitance of the classical Gouy−Chapman model.[16] These predictions were confirmed by molecular simulations[19−23] and experiments.[24−26]

Temperature dependence of EDLs has also attracted much attention recently.[22,25,27−38] The main focus was on neat ILs, whereas IL−solvent mixtures (ILSMs) received less attention. However, ILSMs often have lower viscosity[39,40] (than that of neat ILs) and were shown to have an overall positive effect on the supercapacitor performance.[41−43] Very recently, Gavish et al.[44] introduced a spatiotemporal theoretical framework to study bulk and interfacial phenomena with ILSMs and McEldrew et al.[45] extended the modified Poisson−Fermi theory for highly concentrated (water-in-salt) electrolytes. Here, we use an approach similar in spirit to refs 44 and 45 but we focus on the capacitance and energy storage in double layers with ILSM close to demixing. We unveil a new type of the capacitance shape emerging in such systems and demonstrate that the capacitance and stored energy increase considerably as the system approaches demixing, which can have practical applications.

RESULTS AND DISCUSSION

We place an ILSM at a flat metallic surface at $z = 0$ (Figure 1a) and write for the grand canonical thermodynamic potential of the system

$$\beta\Omega/A = \int_0^\infty dz[\rho_+ \ln(a^3\rho_+) + \rho_- \ln(a^3\rho_-) + \beta f_{ex}(\rho_\pm)] + \int_0^\infty dz\left[cu - \frac{1}{8\pi\lambda_B}\left(\frac{\partial u}{\partial z}\right)^2\right] + \beta K\left\{\int_0^\infty dz\left[\frac{\xi_0^2}{2}\left(\frac{\partial\rho}{\partial z}\right)^2 - \frac{1}{2}\rho^2\right] + \frac{\xi_0}{2}\rho_0^2 - h_1\rho_0\right\} - \beta\mu\int_0^\infty \rho\, dz \quad (1)$$

where $\beta = 1/k_BT$, k_B is the Boltzmann constant, T is the temperature, A is the surface area of the electrode, $\rho_\pm$ are the cation and anion densities, $c = \rho_+ - \rho_-$ is the charge density (per elementary charge e), $\rho = \rho_+ + \rho_-$ is the total ion density, and a is the ion diameter (we assume cations and anions of the same size). The first two terms are the ideal gas entropy, and f_{ex} is the free-energy density due to excluded-volume interactions (see below). The fourth term is the electrostatic energy; here, u is the electrostatic potential in units of thermal voltage ($V_T = k_BT/e$) and $\lambda_B = e^2/(k_BT\varepsilon)$ is the Bjerrum length, where ε is the dielectric constant. To single out the effects related to

Received: October 6, 2018
Revised: December 25, 2018
Published: December 31, 2018

DOI: 10.1021/acs.jpcc.8b09772
J. Phys. Chem. C 2019, 123, 1596−1601

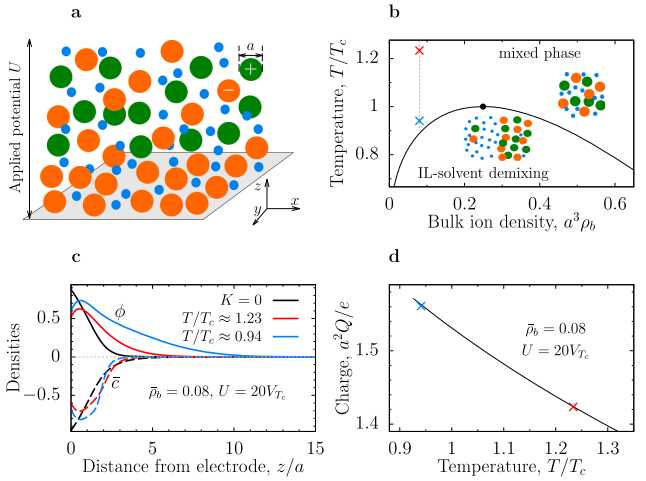

Figure 1. Effect of proximity to demixing on electrical double layers (EDLs). (a) Electrostatic potential U is applied between a flat electrode and the bulk of electrolyte. The ion diameter a is the same for cations (green spheres) and anions (orange spheres). Blue spheres represent the solvent. (b) Bulk phase diagram of an ionic liquid (IL)−solvent mixture predicted by the mean-field model of eq 1. The solid line shows the boundary of the region in which the electrolyte is in the demixed state. The filled circle denotes a (upper) critical point. Temperature is expressed in terms of the critical temperature T_c. The symbols denote the values of T and ρ used in (c), and the thin vertical line shows the value of $a^3\rho_b = 0.08$ used in (d). (c) Order parameter $\phi = a^3(\rho - \rho_b)$, where $\rho = \rho_+ + \rho_-$ is the total ion density (solid lines) and the charge density $\bar{c} = a^3(\rho_+ - \rho_-)$ (dash lines) at various temperatures. The $K = 0$ profiles were obtained by setting $K = 0$ in eq 1. (d) Charge Q per surface area accumulated in the EDL versus temperature. Q is expressed in units of e/a^2 ($\approx 2e/\text{nm}^2 \approx 32\ \mu\text{C/cm}^2$ for the ion diameter $a = 0.7$ nm). The surface field $a^3h_1/\xi_0 = 0.08$ and applied potential $U = 20V_{T_c}$, where thermal voltage $V_{T_c} = k_BT_c/e$ ($k_BT/e \approx 26$ mV at room temperature).

demixing, we assume ε as temperature independent and comment on it later.

Parameter K describes ion−ion and ion−solvent dispersion (van der Waals) interactions and ξ_0 characterizes the spatial extension of these interactions[46,47] (note that K has a unit of energy times volume). The surface term $\xi_0\rho_0^2$, where $\rho_0 = \rho(z = 0)$, arises because of missing neighbors caused by the presence of an electrode, and h_1 is the electrode's ionophilicity: negative h_1 means that an electrode favors solvent, whereas positive h_1 corresponds to an electrode favoring ions (but see below eq 3b), and we assume this preference the same for cations and anions. In the last term, μ is the chemical potential of an ionic liquid with respect to the solvent. Note that eq 1 is also applicable to neat ILs, in which case μ is the bulk chemical potential of ions.

If we set $K = 0$ in eq 1, then our model reduces to the one with pure steric and electrostatic interactions. Such models, with various expressions for f_{ex}, have been extensively studied in the literature.[12,14−18,32,33,48,49] A particularly popular approach is the lattice-gas model, also known as the Bikerman or Kornyshev model in the context of ionic liquids.[16,20,50,51] This model captures well the physics of electrical double layers[19−22] but overestimates steric repulsions.[52] We therefore decided to use the Carnahan−Starling (CS) approximation for the excluded-volume free energy, to give our discussions a more quantitative flavor;[53] the CS free energy is

$$f_{ex}(\rho) = k_BT\rho\left[\frac{4\eta - 3\eta^2}{(1-\eta)^2} - 1\right] \tag{2}$$

where $\eta = \pi a^3\rho/6 = \pi\bar{\rho}/6$ is the ion packing fraction. This choice of f_{ex} in eq 1 describes ILSMs with the ion size larger than that of the solvent so that the solvent can be treated as an effective homogeneous medium (for comparative ion−solvent sizes, the solvent entropy must be explicitly taken into account). Although we focused here on low ion densities, our approach can also be extended to study highly concentrated electrolytes.[45,54,55]

For a bulk system (i.e., without an electrode), eq 1 reduces to $\beta a^3\Omega(\bar{\rho})/V = -\bar{\rho}^2/2\overline{T} + \bar{\rho}\ \ln(\bar{\rho}/2) + \beta f_{ex}(\bar{\rho}) - \beta\mu\bar{\rho}$, where V is the system volume and $\overline{T} = k_BTa^3/K$ is dimensionless temperature. This model predicts demixing phase transitions. The phase diagram consists of a region where solvent and IL are in the demixed state, which shrinks and ends at a (upper) critical point as temperature increases (Figure 1b). We found for the critical density $\rho_ca^3 \approx 0.25$ and temperature $\overline{T}_c \approx 0.09$; the critical density proves to be in good agreement with the experimental values.[56] Since we are interested in temperature-induced effects, we shall use the critical temperature as a reference point and take the temperature-dependent "constants" at T_c.

It turned out convenient to introduce an "order parameter" $\phi = \bar{\rho} - \bar{\rho}_b$, where $\bar{\rho}_b = a^3\rho_b$ is the equilibrium ion density in the bulk. Minimizing eq 1 with respect to ϕ and making use of the bulk condition $c(\infty) = \phi(\infty) = 0$, we found

$$\xi_0^2\phi'' + \phi = \overline{T}[\ \ln(1 + \phi/\bar{\rho}_b) - \ \ln\cosh(u) + \Delta\mu_{ex}] \tag{3a}$$

where primes denote the derivatives with respect to z coordinate and $\Delta\mu_{ex} = \mu_{ex} - \mu_{ex}^b$ with $\mu_{ex} = \beta\partial f_{ex}/\partial\rho$ and $\mu_{ex}^b = \mu_{ex}(z = \infty)$. The boundary conditions are $\phi(\infty) = 0$ and

$$\xi_0\phi'(0) - \phi(0) + \tilde{h}_1 = 0 \tag{3b}$$

where $\tilde{h}_1 = a^3h_1/\xi_0 - \bar{\rho}_b$. The value $\tilde{h}_1 = 0$, which corresponds to $h_1 = \rho_b\xi_0$, means that at no applied potential the surface prefers the same ion density as that in bulk, i.e., $\phi = 0$ and $\rho_0 = \rho_b$. For $h_1 < \rho_b\xi_0$, the preferred IL density at the surface is lower than the bulk value even if the surface is "ionophilic" according to our definition ($h_1 > 0$).

Minimization of eq 1 with respect to u and c yields

$$\lambda_D^2u'' = (1 + \phi/\bar{\rho}_b)\tanh(u) \tag{4}$$

where $\lambda_D = (4\pi\rho_b\lambda_B)^{-1/2}$ is the Debye screening length in bulk electrolyte. The boundary conditions are $u(\infty) = 0$ and $u(0) = eU/k_BT$, where U is the applied potential (Figure 1a).

To study the effect of demixing, we solved the system of eqs 3a, 3b, and 4 numerically for various temperatures and IL concentrations. We took a typical example $\xi_0 = a$ and the Bjerrum length $\lambda_B^c = a$.

Density Profiles and Charge Storage. Figure 1c shows that in the absence of dispersion interactions ($K = 0$ in eq 1), the thickness of the surface layer is comparable to the ion diameter and, at sufficiently high potentials, consists predominantly of counterions. At a finite temperature, the surface layer grows by accumulating more coions so that the total ion density at the electrode increases. This is because dispersion interactions favor higher ion densities, partially compensating the electrostatic repulsions. A small peak developed in ρ and c at short distances arises due to "missing

DOI: 10.1021/acs.jpcc.8b09772
J. Phys. Chem. C 2019, 123, 1596−1601

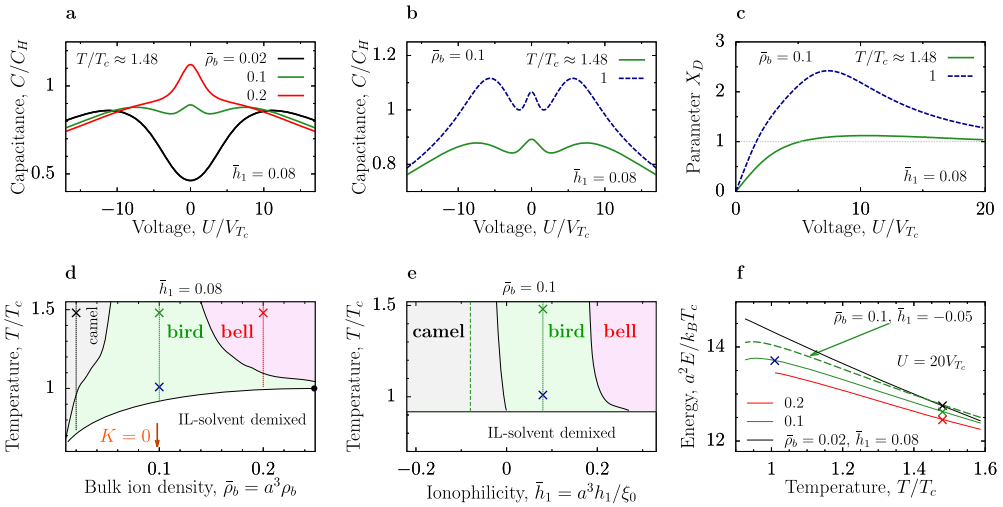

Figure 2. Capacitance and energy storage close to demixing. (a) Differential capacitance as a function of applied potential for constant temperature and various IL concentrations, demonstrating the camel, bird, and bell-shaped capacitances. Voltage is measured in terms of thermal voltage $V_{T_c} = k_BT_c/e$ (≈26 mV at room temperature), and capacitance is measured in unit of $C_H = \varepsilon/4\pi a$ (≈8 μF/cm^2 for a = 0.7 nm with the permittivity of water at room temperature). (b) Effect of temperature on the bird-shaped capacitance. (c) Charging parameter X_D, eq 6, as a function of voltage. (d) Capacitance diagram showing the regions with camel, bird, and bell-like capacitances. The thin vertical lines denote the values of ρ used in (f), and the symbols show the values of the temperature and density used in (a)−(c). The arrow shows the location of the bell-to-camel transformation in the absence of dispersion forces (K = 0 in eq 1). (e) Capacitance diagram in the plane of temperature and electrode's ionophilicity (surface field $\bar{h}_1 = a^3h_1/\xi_0$). (f) Stored energy per surface area as a function of temperature for various IL concentrations and surface fields at an applied potential of $U = 20V_{T_c}$. Energy density is measured in units of $E_T = k_BT/a^2$ (≈0.84 μJ/cm^2 ≈ 0.23 nW h/cm^2 for a = 0.7 nm at room temperature).

neighbors" created by the electrode (the $\xi_0\rho_0^2$ term in eq 1); clearly, this is not captured by the pure steric-electrostatic model (K = 0 in Figure 1c).

In the vicinity of demixing, dispersion forces begin to play an increasingly important role and the surface layer grows to become macroscopically thick, reminiscent of electrowetting. Remarkably, the charge accumulated in an EDL, $Q = e\int_0^\infty c(z)\,dz$, increases as the temperature decreases toward demixing (Figure 1d), which may have practical applications.

Capacitance and Charging Mechanisms. An important characteristic of EDLs is differential capacitance

$$C(U) = \frac{dQ}{dU} \tag{5}$$

Figure 2a shows that $C(U)$ can have multiple peaks as a function of an applied potential U, depending on the IL concentration. The case of low concentrations was extensively studied in the literature.[12,14−22] In accord with the previous work, here we observed a so-called camel-shaped capacitance (the $\bar{\rho}$ = 0.02 curve in Figure 2a), i.e., a minimum at the potential of zero charge (PZC) and two symmetric maxima. At a high density, we obtained a bell-shaped capacitance, which exhibits a single peak at the PZC and decreases monotonically for increasing voltage. Also, this behavior was well studied theoretically[12,14−22] and by experiments.[24−26]

However, our calculations revealed that the capacitance can exhibit three peaks at intermediate IL concentrations. The first peak is at the PZC, characteristic of high densities, whereas the two other peaks at the positive and negative potentials bear a resemblance to the camel-shaped capacitance. Inspired by Kornyshev's bells and camels,[16] we shall call it a bird-shaped capacitance, in view of the similarity of its shape to a flying bird (Figure 2b).

To achieve a deeper insight into the charging process close to demixing, we calculated the charging parameter[57,58]

$$X_D(U) = \frac{e}{C(U)}\frac{d\Gamma}{dU} \tag{6}$$

where $\Gamma = \int_0^\infty \phi(z)\,dz$ is the surface coverage (by an ionic liquid). $X_D(U) = 0$ means that, at a potential U, the charging is due to swapping coions for counterions. $X_D = 1$ corresponds to counterion electrosorption (or simply adsorption), and $X_D > 1$ implies that both counterions and coions are adsorbed into the surface layer; a negative X_D means desorption of ions from the surface layer.

Far from demixing, charging mechanisms are qualitatively similar for all three types of capacitance (for a typical curve, see the green line in Figure 2c). However, we found that approaching demixing has a vivid effect on the charging mechanisms and capacitance. In particular, for a birdlike capacitance, the capacitance increases and its shape becomes more pronounced (Figure 2b). The enhanced capacitance is due to the increased ion density at the surface occurring close to demixing (Figure 1c), and this is reflected in the charging parameter, which becomes significantly greater than unity (Figure 2c).

The diagram in Figure 2d shows the regions in which our theory predicted the camel, bird, and bell-shaped capacitances. Remarkably, the bird-shaped capacitance occupies a relatively large domain, which extends upon approaching the line of demixing transitions. The transformation between different types of capacitance can be induced by changing temperature or concentration.

In the absence of dispersion forces (K = 0 in eq 1), a transformation between the camel and bell shapes was found at $\rho_b = \rho_{b,1} \approx 0.098a^{-3}$ (the arrow in Figure 2d; there is no bird-shaped capacitance for K = 0). This means that the bird-shaped capacitance can emerge either from the camel shape by developing another hump or by developing two wings in the bell shape. In the former case, a hump appears at u = 0 if an electrode is sufficiently ionophilic to keep a high ion density at

DOI: 10.1021/acs.jpcc.8b09772
J. Phys. Chem. C 2019, 123, 1596−1601

the electrode. Referring to Figure 2d, $\tilde{h}_1$ in eq 3b increases as the bulk ion density, ρ_b, is reduced and so the electrode can maintain a high density in its vicinity also for $\rho_b < \rho_{b,1}$.

The appearance of wings in the bell-shaped capacitance is more interesting and can be related to electrowetting-like phenomena and charging mechanisms. Figure 2c demonstrates that X_D develops a peak at $u = u_1$ ($\approx 6V_{T_c}$), whose value can be well above unity. This means that both counter and coions enter the surface layer in response to the applied potential. The increased ion density at the electrode enhances ionic screening and leads to a peak in the capacitance at $u \approx u_1$ (Figure 2b).

Figure 2e shows that, at a fixed ion concentration, the capacitance shape can be changed by varying the affinity of electrodes toward ions, controlled by the parameter h_1. An ionophobic electrode (low or negative h_1) favors the camel shape, and a strongly ionophilic electrode produces the bell shape. The bird shape emerges in the intermediate regime, defining the border zone between ionophilic and ionophobic.

It is interesting to note that Alam et al.[59] have observed experimentally the appearance of humps at the potential of zero charge in the parabolic capacitance−voltage curves for some N_2-saturated room-temperature ILs; the cause of this appearance was unknown.[59] Our theory suggests that it is related to IL−electrode wetting properties, with the humps appearing for ILs with higher affinity for electrodes (Figure 2e); clearly, this effect cannot be captured by the pure steric-electrostatic theories.

The emergence of wings in the bell-shaped capacitance has been observed[60] in molecular dynamics simulations of neat 1-butyl-3-methylimidazolium hexafluorophosphate (commonly known as BMIM-PF_6) on a gold surface; also this behavior was not rationalized. Our analysis suggests that it is likely related to a voltage-triggered adsorption of ions at the electrode at intermediate voltages, as manifested by the charging parameter X_D (Figure 2c).

Energy Storage. We next calculated the energy density stored in an EDL, $E(U) = \int_0^U C(u)u\,du$. Figure 2f shows that E increases significantly as the system approaches demixing. Such an enhanced energy storage is consistent with the increased capacitance (Figure 2b) and accumulated charge (Figure 1d). Interestingly, the largest enhancement was obtained at low IL concentrations. In this case, the applied potential has a stronger effect on the near-surface structure, providing a comparably higher increase of the IL density at the electrode for decreasing temperature. Similarly as in nanoconfinement,[61−63] making an electrode ionophobic enhances the energy storage, but the relative increase of the energy obtained by decreasing temperature is comparable to that of the ionophilic electrode (the solid and dashed green lines in Figure 2f).

For many ILSMs, the demixing critical temperature, T_c, is in the range of 300−400 K,[56,64,65] which means that $\Delta T = 0.1T_c$ corresponds to 30−40 K. Figure 2f suggests that the energy stored in an EDL changes significantly in this temperature range, which can be used to generate electricity from waste heat. This can be done, for instance, by using a capacitor with ILSM close to demixing as a "buffer" capacitor to be charged from a "permanent" storage (battery) when a device is heated up (to T_h) and to discharge it back to the permanent storage when it cools down (other realizations are also possible). Then, for a temperature jump $\Delta T = 0.1T_c$ and taking $T_h = T_c$, we estimated the energy gain ΔE to be about 0.1 nW h/cm^2 at $U = 20V_{T_c} \approx 0.5$ V for $a^3\rho = 0.02$ (about 0.095 M for ion diameter $a = 0.7$ nm; note that the density is off critical and the ILSM is in the mixed state during the whole cycle). Taking a macroporous electrode with a modest 100 m^2/g surface area, we obtained the gain from a single cycle $\Delta E \approx 0.1$ W h/kg.

We recall now that we deliberately did not take into account the temperature variation of the dielectric constant, ε, which can be significant for polar solvents. It is not difficult to see, however, that in doing so we underestimated ΔE. Taking the Gouy−Chapman capacitance for simplicity, one finds that $C \sim \varepsilon^{1/2}$ increases as ε increases for decreasing temperature, and hence ΔE shall increase correspondingly. We confirmed by explicit numerical calculations that this is indeed the case; the details will be published elsewhere.

Finally, we stress that our heat-to-electricity converter (HTEC) differs from other HTECs, which rely on enhancing Faraday processes[34] or increasing voltage[32,33] for increasing temperature. In contrast to them, the demixing-based HTECs exploit the collective behavior and metastability of an IL-rich phase close to demixing, which leads to the rise of capacitance and energy storage.

CONCLUSIONS

We have studied electrical double layers (EDLs) with ionic liquid−solvent mixtures close to demixing. We revealed the emergence of a bird-shaped capacitance, in addition to the well-known bell and camel shapes. The camel and bell shapes appear for ionophobic and ionophilic electrodes, respectively, while the bird shape separates these two extremes; this suggests that the capacitance shape may serve as an electrochemical signature of the electrode's affinity for ions. Our findings suggest a plausible explanation for the appearance of humps in the capacitance−voltage curves observed for some water and N_2-saturated room-temperature ionic liquids.[59] We also demonstrated that EDLs experience vivid changes upon approaching ionic liquid−solvent demixing at low concentrations. Particularly, the energy stored in an EDL can be considerably enhanced, which can be utilized to generate electricity from heat.

AUTHOR INFORMATION

Corresponding Author

*E-mail: svyatoslav.kondrat@gmail.com, skondrat@ichf.edu.pl, aciach@ichf.edu.pl.

ORCID

Enrique Lomba: 0000-0002-4768-2040

Svyatoslav Kondrat: 0000-0003-4448-0686

Notes

The authors declare no competing financial interest.

ACKNOWLEDGMENTS

This work was supported by the European Unions Horizon 2020 research and innovation programmes under the Marie Skłodowska-Curie grant agreement No. 711859 to C.C. and No. 734276 to A.C. and S.K. Additional funding was received from the Ministry of Science and Higher Education of Poland for the project No. 734276 in the years 2017−2018 (agreement No. 3854/H2020/17/2018/2) and for the implementation of the international co-financed project No. 711859 in the years 2017−2021. S.K. thanks Huazhong University of Science and Technology (HUST, Wuhan, China) for hospitality during his visit to HUST, where part of this

DOI: 10.1021/acs.jpcc.8b09772
J. Phys. Chem. C 2019, 123, 1596−1601

work has been done. We are grateful to Mathijs Janssen (MPI-IS, Stuttgart) and Guang Feng (HUST) for critical reading of the manuscript and insightful comments.

REFERENCES

(1) Welton, T. Room-temperature ionic liquids. solvents for synthesis and catalysis. *Chem. Rev.* **1999**, *99*, 2071−2084.
(2) Fedorov, M. V.; Kornyshev, A. A. Ionic liquids at electrified interfaces. *Chem. Rev.* **2014**, *114*, 2978−3036.
(3) MacFarlane, D. R.; Tachikawa, N.; Forsyth, M.; Pringle, J. M.; Howlett, P. C.; Elliott, G. D.; Davis, J. H.; Watanabe, M.; Simon, P.; Angell, C. A. Energy applications of ionic liquids. *Energy Environ. Sci.* **2014**, *7*, 232−250.
(4) Watanabe, M.; Thomas, M. L.; Zhang, S.; Ueno, K.; Yasuda, T.; Dokko, K. Application of ionic liquids to energy storage and conversion materials and devices. *Chem. Rev.* **2017**, *117*, 7190−7239.
(5) Salanne, M. Ionic liquids for supercapacitor applications. *Top. Curr. Chem.* **2017**, *375*, 63.
(6) Martins, V. L.; Torresi, R. M. Ionic liquids in electrochemical energy storage. *Curr. Opin. Electrochem.* **2018**, *9*, 26−32.
(7) Perkin, S. Ionic liquids in confined geometries. *Phys. Chem. Chem. Phys.* **2012**, *14*, 5052−5062.
(8) *Catalysis in Ionic Liquids*; Hardacre, C.; Parvulescu, V., Eds.; Royal Society of Chemistry, 2014.
(9) Itoh, T. Ionic liquids as tool to improve enzymatic organic synthesis. *Chem. Rev.* **2017**, *117*, 10567−10607.
(10) Conway, B. E. *Electrochemical Capacitors: Scientific Fundamentals and Technological Applications*; Kluwer, 1999.
(11) Kralj-Iglič, V.; Iglič, A. A simple statistical mechanical approach to the free energy of the electric double layer including the excluded volume effect. *J. Phys. II France* **1996**, *6*, 477−491.
(12) Borukhov, I.; Andelman, D.; Orland, H. Steric effects in electrolytes: A modified Poisson-Boltzmann equation. *Phys. Rev. Lett.* **1997**, *79*, 435−438.
(13) Bohinc, K.; Kralj-Iglič, V.; Iglič, A. Thickness of electrical double layer. Effect of ion size. *Electrochim. Acta* **2001**, *46*, 3033−3040.
(14) Di Caprio, D.; Borkowska, Z.; Stafiej, J. Simple extension of the Gouy-Chapman theory including hard sphere effects. Diffuse layer contribution to the differential capacity curves for the electrode − electrolyte interface. *J. Electroanal. Chem.* **2003**, *540*, 17−23.
(15) Di Caprio, D.; Borkowska, Z.; Stafiej, J. Specific ionic interactions within a simple extension of the Gouy-Chapman theory including hard sphere effects. *J. Electroanal. Chem.* **2004**, *572*, 51−59.
(16) Kornyshev, A. Double-layer in ionic liquids: Paradigm change? *J. Phys. Chem. B* **2007**, *111*, 5545−5557.
(17) Kilic, M. S.; Bazant, M. Z.; Ajdari, A. Steric effects in the dynamics of electrolytes at large applied voltages. I. Double-layer charging. *Phys. Rev. E* **2007**, *75*, No. 021502.
(18) Oldham, K. B. A Gouy-Chapman-Stern model of the double layer at a (metal)/(ionic liquid) interface. *J. Electroanal. Chem.* **2008**, *613*, 131−138.
(19) Fedorov, M. V.; Kornyshev, A. A. Towards understanding the structure and capacitance of electrical double layer in ionic liquids. *Electrochim. Acta.* **2008**, *53*, 6835.
(20) Fedorov, M. V.; Kornyshev, A. A. Ionic liquid near a charged wall: Structure and capacitance of electrical double layer. *J. Phys. Chem. B* **2008**, *112*, 11868−11872.
(21) Georgi, N.; Kornyshev, A. A.; Fedorov, M. V. The anatomy of the double layer and capacitance in ionic liquids with anisotropic ions: Electrostriction vs lattice saturation. *J. Electroanal. Chem.* **2010**, *649*, 261.
(22) Vatamanu, J.; Borodin, O.; Smith, G. D. Molecular simulations of the electric double layer structure, differential capacitance and charging kinetics for the n-methyl-n-propylpyrrolidinium bis-fluorosulfonyl imide at graphite electrodes. *J. Phys. Chem. B* **2011**, *115*, 3073−3084.
(23) Breitsprecher, K.; Košovan, P.; Holm, C. Coarse-grained simulations of an ionic liquid-based capacitor: I. Density, ion size, and valency effects. *J. Phys.: Condens. Matter* **2014**, *26*, No. 284108.
(24) Alam, M. T.; Islam, M. M.; Okajima, T.; Ohsaka, T. Measurements of differential capacitance at mercury/room-temperature ionic liquids interfaces. *J. Phys. Chem. C* **2007**, *111*, 18326−18333.
(25) Lockett, V.; Sedev, R.; Ralston, J.; Horne, M.; Rodopoulos, T. Differential capacitance of the electrical double layer in imidazolium-based ionic liquids: Influence of potential, cation size, and temperature. *J. Phys. Chem. C* **2008**, *112*, 7486−7495.
(26) Islam, M. M.; Alam, M. T.; Okajima, T.; Ohsaka, T. Electrical double layer structure in ionic liquids: An understanding of the unusual capacitance-potential curve at a nonmetallic electrode. *J. Phys. Chem. C* **2009**, *113*, 3386−3389.
(27) Holovko, M.; Kapko, V.; Henderson, D.; Boda, D. On the influence of ionic association on the capacitance of an electrical double layer. *Chem. Phys. Lett.* **2001**, *341*, 363−368.
(28) Reszko-Zygmunt, J.; Sokołowski, S.; Henderson, D.; Boda, D. Temperature dependence of the double layer capacitance for the restricted primitive model of an electrolyte solution from a density functional approach. *J. Chem. Phys.* **2005**, *122*, No. 084504.
(29) di Caprio, D.; Valiskó, M.; Holovko, M.; Boda, D. Anomalous temperature dependence of the differential capacitance in valence asymmetric electrolytes. Comparison of Monte Carlo simulation results and the field theoretical approach. *Mol. Phys.* **2006**, *104*, 3777−3786.
(30) Schiffer, J.; Linzen, D.; Sauer, D. U. Heat generation in double layer capacitors. *J. Power Sources* **2006**, *160*, 765−772.
(31) Drüschler, M.; Borisenko, N.; Wallauer, J.; Winter, C.; Huber, B.; Endres, F.; Roling, B. New insights into the interface between a single-crystalline metal electrode and an extremely pure ionic liquid: Slow interfacial processes and the influence of temperature on interfacial dynamics. *Phys. Chem. Chem. Phys.* **2012**, *14*, 5090.
(32) Janssen, M.; Härtel, A.; van Roij, R. Boosting capacitive blue-energy and desalination devices with waste heat. *Phys. Rev. Lett.* **2014**, *113*, No. 268501.
(33) Härtel, A.; Janssen, M.; Weingarth, D.; Presser, V.; van Roij, R. Heat-to-current conversion of low-grade heat from a thermocapacitive cycle by supercapacitors. *Energy Environ. Sci.* **2015**, *8*, 2396−2401.
(34) Wang, J.; Feng, S.-P.; Yang, Y.; Hau, N. Y.; Munro, M.; Ferreira-Yang, E.; Chen, G. "Thermal charging" phenomenon in electrical double layer capacitors. *Nano Lett.* **2015**, *15*, 5784−5790.
(35) Ivaništšev, V. B.; Kirchner, K.; Fedorov, M. V. Double Layer in Ionic Liquids: Capacitance vs Temperature, arXiv:1711.06854 [cond-mat.soft]. arXiv.org e-Print archive. http://arxiv.org/abs/1711.06854v1 (submitted Nov 18, 2017).
(36) Janssen, M.; van Roij, R. Reversible heating in electric double layer capacitors. *Phys. Rev. Lett.* **2017**, *118*, No. 096001.
(37) Janssen, M.; Griffioen, E.; Biesheuvel, P. M.; van Roij, R.; Erné, B. Coulometry and calorimetry of electric double layer formation in porous electrodes. *Phys. Rev. Lett.* **2017**, *119*, No. 166002.
(38) Chen, M.; Goodwin, Z. A. H.; Feng, G.; Kornyshev, A. A. On the temperature dependence of the double layer capacitance of ionic liquids. *J. Electroanal. Chem.* **2018**, *819*, 347−358.
(39) Chaban, V. V.; Voroshylova, I. V.; Kalugin, O. N.; Prezhdo, O. V. Acetonitrile boosts conductivity of imidazolium ionic liquids. *J. Phys. Chem. B* **2012**, *116*, 7719−7727.
(40) Rilo, E.; Vila, J.; García-Garabal, S.; Varela, L. M.; Cabeza, O. Electrical conductivity of seven binary systems containing 1-ethyl-3-methyl imidazolium alkyl sulfate ionic liquids with water or ethanol at four temperatures. *J. Phys. Chem. B* **2013**, *117*, 1411−1418.
(41) Lin, R.; Huang, P.; Ségalini, J.; Largeot, C.; Taberna, P. L.; Chmiola, J.; Gogotsi, Y.; Simon, P. Solvent effect on the ion adsorption from ionic liquid electrolyte into sub-nanometer carbon pores. *Electrochim. Acta* **2009**, *54*, 7025−7032.
(42) Jiang, D. E.; Jin, Z.; Henderson, D.; Wu, J. Solvent effect on the pore-size dependence of an organic electrolyte supercapacitor. *J. Phys. Chem. Lett.* **2012**, *3*, 1727−1731.

DOI: 10.1021/acs.jpcc.8b09772
J. Phys. Chem. C 2019, 123, 1596−1601

(43) Burt, R.; Breitsprecher, K.; Daffos, B.; Taberna, P.-L.; Simon, P.; Birkett, G.; Zhao, X. S.; Holm, C.; Salanne, M. Capacitance of nanoporous carbon-based supercapacitors is a trade-off between the concentration and the separability of the ions. *J. Phys. Chem. Lett.* **2016**, *7*, 4015−4021.
(44) Gavish, N.; Elad, D.; Yochelis, A. From solvent-free to dilute electrolytes: Essential components for a continuum theory. *J. Phys. Chem. Lett.* **2018**, *9*, 36−42.
(45) McEldrew, M.; Goodwin, Z. A. H.; Kornyshev, A. A.; Bazant, M. Z. Theory of the double layer in water-in-salt electrolytes. *J. Phys. Chem. Lett.* **2018**, 5840−5846.
(46) Ciach, A.; Stell, G. Effect of competition between Coulomb and dispersion forces on phase transitions in ionic systems. *J. Chem. Phys.* **2001**, *114*, 3617−3630.
(47) Pousaneh, F.; Ciach, A.; Maciołek, A. Effect of ions on confined near-critical binary aqueous mixture. *Soft Matter* **2012**, *8*, 7567.
(48) Bazant, M. Z.; Storey, B. D.; Kornyshev, A. A. Double layer in ionic liquids: Overscreening versus crowding. *Phys. Rev. Lett.* **2011**, *106*, No. 046102.
(49) Lee, A. A.; Kondrat, S.; Vella, D.; Goriely, A. Dynamics of ion transport in ionic liquids. *Phys. Rev. Lett.* **2015**, *115*, No. 106101.
(50) Bikerman, J. XXXIX. Structure and capacity of electrical double layer. *London, Edinburgh Dublin Philos. Mag. J. Sci.* **1942**, *33*, 384−397.
(51) Bazant, M. Z.; Kilic, M. S.; Storey, B. D.; Ajdari, A. Towards an understanding of induced-charge electrokinetics at large applied voltages in concentrated solutions. *Adv. Colloid Interface Sci.* **2009**, *152*, 48.
(52) Antypov, D.; Barbosa, M. C.; Holm, C. Incorporation of excluded-volume correlations into Poisson−Boltzmann theory. *Phys. Rev. E* **2005**, *71*, No. 061106.
(53) López-García, J. J.; Horno, J.; Grosse, C. Differential capacitance of the diffuse double layer at electrode-electrolyte interfaces considering ions as dielectric spheres: Part I. Binary electrolyte solutions. *J. Colloid Interface Sci.* **2017**, *496*, 531−539.
(54) Vatamanu, J.; Borodin, O. Ramifications of water-in-salt interfacial structure at charged electrodes for electrolyte electrochemical stability. *J. Phys. Chem. Lett.* **2017**, *8*, 4362−4367.
(55) Li, Z.; Jeanmairet, G.; Méndez-Morales, T.; Rotenberg, B.; Salanne, M. Capacitive performance of water-in-salt electrolytes in supercapacitors: A simulation study. *J. Phys. Chem. C* **2018**, *122*, 23917−23924.
(56) Rotrekl, J.; Storch, J.; Velíšek, P.; Schröer, W.; Jacquemin, J.; Wagner, Z.; Husson, P.; Bendová, M. Liquid phase behavior in systems of 1-butyl-3-alkylimidazolium bis{(trifluoromethyl)sulfonyl}-imide ionic liquids with water: Influence of the structure of the c5 alkyl substituent. *J. Solution Chem.* **2017**, *46*, 1456−1474.
(57) Forse, A. C.; Merlet, C.; Griffin, J. M.; Grey, C. P. New perspectives on the charging mechanisms of supercapacitors. *J. Am. Chem. Soc.* **2016**, *138*, 5731−5744.
(58) Breitsprecher, K.; Abele, M.; Kondrat, S.; Holm, C. The effect of finite pore length on ion structure and charging. *J. Chem. Phys.* **2017**, *147*, No. 104708.
(59) Alam, M. T.; Islam, M. M.; Okajima, T.; Ohsaka, T. Capacitance measurements in a series of room-temperature ionic liquids at glassy carbon and gold electrode interfaces. *J. Phys. Chem. C* **2008**, *112*, 16600−16608.
(60) Sha, M.; Dou, Q.; Luo, F.; Zhu, G.; Wu, G. Molecular insights into the electric double layers of ionic liquids on au(100) electrodes. *ACS Appl. Mater. Interfaces* **2014**, *6*, 12556−12565.
(61) Kondrat, S.; Kornyshev, A. Pressing a spring: What does it take to maximize the energy storage in nanoporous supercapacitors? *Nanoscale Horiz.* **2016**, *1*, 45−52.
(62) Lee, A. A.; Vella, D.; Goriely, A.; Kondrat, S. The capacitance-power-hysteresis trilemma in nanoporous supercapacitors. *Phys. Rev. X* **2016**, *6*, No. 021034.
(63) Lian, C.; Liu, H.; Henderson, D.; Wu, J. Can ionophobic nanopores enhance the energy storage capacity of electric-double-layer capacitors containing nonaqueous electrolytes? *J. Phys.: Condens. Matter* **2016**, *28*, No. 414005.
(64) Butka, A.; Vale, V. R.; Saracsan, D.; Rybarsch, C.; Weiss, V. C.; Schröer, W. Liquid-liquid phase transition in solutions of ionic liquids with halide anions: Criticality and corresponding states. *Pure Appl. Chem.* **2008**, *80*, 1613−1630.
(65) Crosthwaite, J. M.; Aki, S. N. V. K.; Maginn, E. J.; Brennecke, J. F. Liquid phase behavior of imidazolium-based ionic liquids with alcohols. *J. Phys. Chem. B* **2004**, *108*, 5113−5119.

DOI: 10.1021/acs.jpcc.8b09772
J. Phys. Chem. C 2019, 123, 1596−1601